ACS OMEGA

http://pubs.acs.org/journal/acsodf

Article

Silver Nanowires Coated Nitrocellulose Paper for High-Efficiency Electromagnetic Interference Shielding

Raghunath Sahoo, Ramaprabhu Sundara, and Subramanian Venkatachalam*

Cite This: *ACS Omega* 2022, 7, 41426−41436

Read Online

ACCESS | Metrics & More | Article Recommendations | Supporting Information

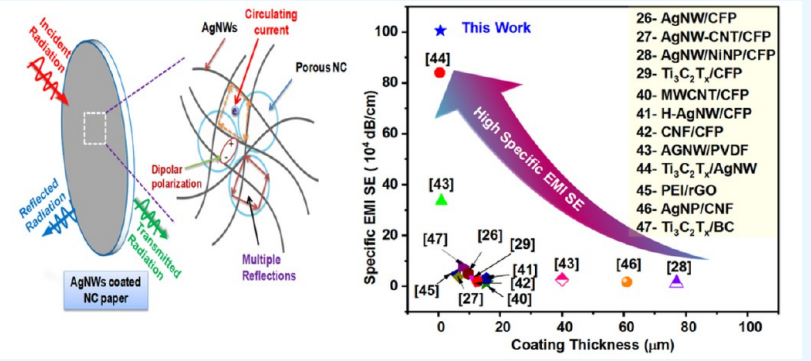

ABSTRACT: A thin and conductive coating on an environmentally friendly polymer is imperative for protecting sensitive electronic devices. In this regard, a series of silver nanowires (AgNWs) coated nitrocellulose (NC) papers are fabricated by a simple and fast processed vacuum-assisted filtration method by varying filtrate volume to address electromagnetic interference. Their structural and EMI shielding performance is analyzed. The submicron thick and the lighter paper reveal the conductive AgNWs interwoven on the rough NC surface, making a 2D in-planar structure. Due to a strongly interconnected network, the coated paper displays an exceptional electrical conductivity of 8603 S/m. Despite having a minimum AgNW coating thickness of ∼0.69 μm and an area density of 0.041 mg/cm^2, an ultrahigh EMI shielding effectiveness (SE) of about 69.4 dB (a specific EMI SE (SE/t) of 1005797 dB/cm) in the entire X-band (8−12 GHz) region is achieved. The effective material parameters, extracted using plane-wave theory, indicate that AgNWs form closed current loops resulting in magnetic losses. These AgNWs coated NC papers synthesized by a simple procedure are promising EMI shielding materials for current emerging electronic devices.

1. INTRODUCTION

With the proliferation of application potential for high-frequency electronic devices and communication equipment, the need to tackle electromagnetic pollution, generally caused by electrostatic discharge and electromagnetic interference (EMI), is rising. Electromagnetic interference consisting of electric and magnetic radiations causes the degradation or malfunctioning of nearby devices.[1,2] Also, EMI can be a reason for human health degradation, causing physical and psychological effects that include headache, dizziness, sleep disturbance, depression, and anxiety disorder. More exposure to these radiations can increase the risk of cancer, male infertility, and neurobehavioral disorder.[3,4] Metallic shields have been used for EMI shielding as they reflect electromagnetic radiation (EM) entirely due to their high electrical conductivity. Though metals have excellent mechanical properties, their usage is limited due to their high density, high corrosiveness, low mechanical flexibility, and high processing cost. More specifically, a shield with low density, lightweight, minimal thickness, and absorption-dominated EMI attenuation is the need of the hour.[5,6] The above problems can be solved using conductive polymer composites (CPCs) by dispersing conductive nanofillers in the insulating matrix.[7−9] Among the various nanofillers, the families of 1D nanomaterials such as nanotubes, nanowires, and nanofibers are extensively preferred over 0D nanoparticles for reinforcing in the insulating polymer matrix due to their exceptional intrinsic electrical conductivity and formation of conductive pathways inside the polymer matrix even at a lower percolation.[10−15] Due to high electrical conductivity, good flexibility, and high aspect ratio, AgNWs are suitable candidates over others.[16] Yu et al. investigated the polymer composites with AgNWs as a nanofiller in both hydrophilic poly(vinyl alcohol) and hydrophobic epoxy matrix.[17] The study showed that AgNWs are 4

Received: August 13, 2022
Accepted: October 4, 2022
Published: November 1, 2022

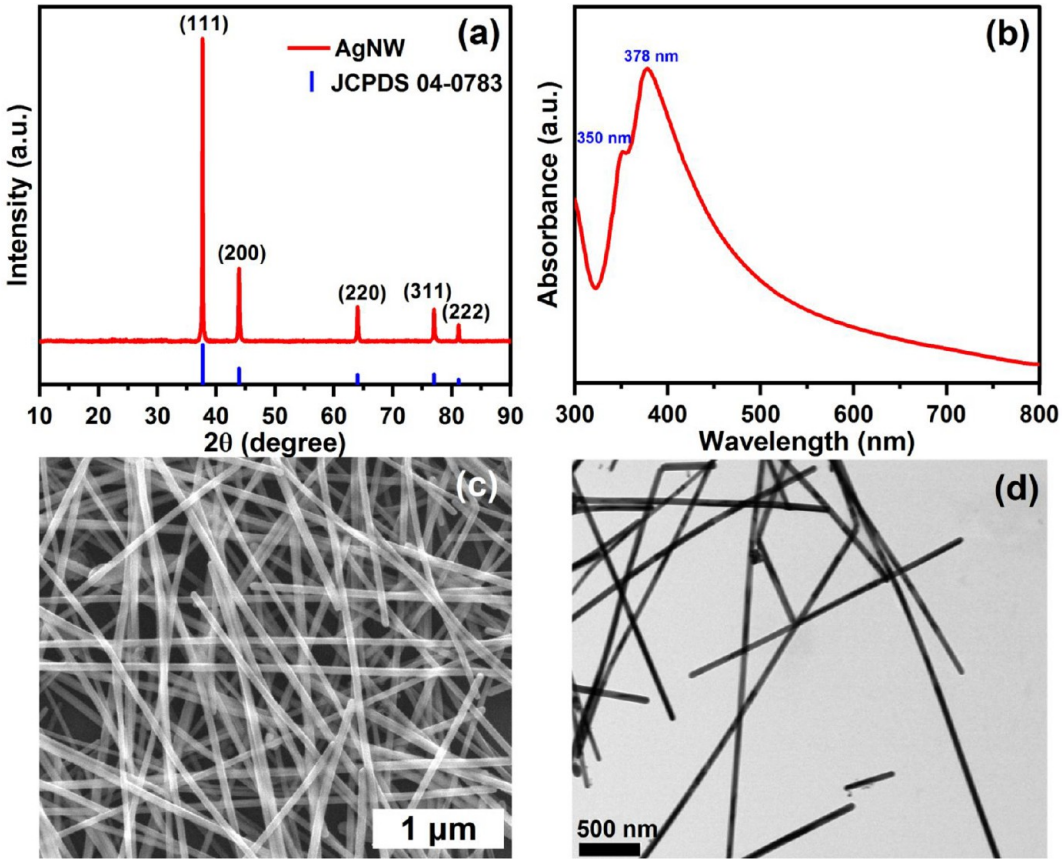

Figure 1. Structural and morphological characterizations of as-synthesized AgNWs; (a) XRD pattern, (b) UV−vis Spectra, (c) FESEM image, and (d) TEM image.

times more effective than silver nanoparticles (AgNPs). After this result, researchers have fabricated poly(ethersulfones)/AgNWs/poly(ethylene terephthalate),[18] AgNWs/polyamide,[19] AgNWs/polyaniline,[20] AgNWs/polystyrene,[21] and so on. However, the large content of AgNWs in the polymer composites leads to high cost and, thus, inhibits the scaling industrially.

Eco-friendly polymer substrates such as cellulose and its derivatives have been used as substrates for EMI shielding applications due to their abundance, biodegradability, and nontoxic nature. Liang et al. used cotton cellulose to fabricate vacuum-assisted free-standing AgNW (50 wt %)-cellulose 44.5 μm thick film displaying exceptional EMI Shielding effectiveness (SE) of 101 dB.[22] Similarly, Chen et al. developed wood pulp-derived cellulose nanofiber (CNF)/ AgNW 40 μm thick free-standing film by vacuum filtration and peeling, which exhibited an EMI SE of 39.3 dB in X-band with a high AgNW content of 14.3 vol %.[23] An asymmetric sandwiched structure consisting of 50 wt % of $Ti_3C_2T_x$-AgNW in carboxyl cellulose nanofibers matrix showed EMI SE of about 55.9 dB.[24] Liu et al. used 5 wt % AgNW in cellulose nanofibril to fabricate 50 μm thick paper by a step-by-step self-assembly process, which exhibited 67.2 dB in the X-band.[25] However, all these free-standing films use higher AgNW loading, which affects the cost and scalability. Lee et al. fabricated a AgNW-cellulose filter paper (CFP) composite using the dip-coating method to achieve an EMI SE of 48.1 dB at a lower 0.53 vol % showing the effectiveness of cellulose composite paper in forming a conductive network.[26] Choi et al. suggested the addition of CNTs on AgNW-cellulose composite paper due to their high oxidation and corrosion resistance. The conductive composite paper exhibited 24.1 dB at 1 GHz with a thin coating thickness (~6.6 μm).[27] Zhan et al. sputter-coated nickel nanoparticles (NiNPs) onto AgNW-coated cellulose composite paper for EMI shielding.[28] At an AgNW content of 0.109 vol % and a NiNP content of 0.013 mg/cm^2, the 77 μm thick composite paper exhibited an EMI SE of 88.4 dB. All these fabrication processes are time-consuming and monotonous. To overcome this hindrance, Zhan et al. suggested a simple and cost-effective vacuum-assisted filtration coating of $Ti_3C_2T_x$ on cellulose filter paper. The one-sided coated 12 μm thick filter paper yielded an EMI SE of 29.1 dB with a volume content of $Ti_3C_2T_x$ of 0.72%.[29] Even after forming a well-aligned structure, it fails to reach optimal EMI SE performance. For miniaturized electronic devices, it is essential to fabricate a submicron thick coated EMI shield with less filler content that can achieve more than 50 dB to eliminate the threat of EMI interference, which remains a significant challenge to achieve.

Conversely, cellulose nitrate or nitrocellulose (NC) is an environmentally friendly polymer formed by treating cellulose with sulfuric acid and nitric acid.[30] While cellulose paper has been studied extensively in the previous literature for EMI shielding application, the EMI shielding performance of NC paper has not been investigated yet to the best of our knowledge. NC filter paper which possesses a highly porous nature and a corrugated (rough) surface, can be a better substrate than cellulose filter paper for strong adhesion and deposition of a flexible and random network of AgNWs.[31] The porous nature of the NC paper might help in forming a porous network of AgNW, giving rise to multiple scattering of EM

https://doi.org/10.1021/acsomega.2c05204
ACS Omega 2022, 7, 41426−41436

radiation that improves both reflection and absorption to enhance the overall EMI shielding performance.

Inspired by the one-sided coating by the vacuum-assisted filtration method, a submicron thick layer of well-connected AgNWs was constructed on one side of the NC filter paper. The structural and electrical properties were characterized. The shielding performance was measured in the X-band frequency region (8−12 GHz) and analyzed further to extract material properties.

2. RESULTS AND DISCUSSION

2.1. Characterization of As-Synthesized Silver Nanowires. Figure 1a presents the XRD of AgNWs, confirming the crystalline nature. The ratio between the intensity of (111) and (200) diffraction planes is about 3.47, which is more than the theoretically predicted value of 2.5, showing the dominance of growth direction along the (111) crystalline plane.[32] PVP plays an essential role in the anisotropic growth of nanowires along the (111) plane. The lattice constant of the crystalline nanowires is calculated to be around 4.089 Å which nearly matches the lattice constant of silver (4.086 Å) having JCPDS file no. 04−0783. Figure 1b depicts the absorbance obtained from the UV−vis spectrum. A sharper peak at 378 nm corresponds to the transverse resonance peak of pentagonally twinned AgNWs. A shoulder peak at 350 nm corresponds to the longitudinal plasmon resonance mode of bulk silver.[33]

Panels c and d of Figures 1 depict the morphology of the silver nanowires. The diameter and length of the nanowires are calculated by measuring over 100 nanowires using the software ImageJ. The average diameter of the nanowires is calculated to be around 53 ± 12 nm, while the average length is around 23 ± 8 μm, extending up to 43 μm and making the aspect ratio of the nanowires to be 437 as shown in Figure S3. Study shows that using long and thin nanowires reduces the number/density of nanowires required for percolative networks and thus effectively enhances the conductivity.[34] The elemental composition of the nanowires is studied by taking the energy dispersive X-ray (EDX) spectra of the nanowires, as shown in Figure S4a. The results reaffirm the presence of high-purity silver (94%) and the rest of the oxygen due to the presence of the capped PVP molecule. The SAED pattern obtained from the TEM images of the nanowires shows diffraction rings of (111), (200), (220), and (311) planes, as shown in Figure S4b.

2.2. Characterization of the Coated NC Paper. *2.2.1. Structural Characterization.* XRD patterns of the AgNWs coated NC paper are studied and analyzed for elemental composition and phase. The XRD pattern obtained for neat NC exhibits an amorphous nature with no prominent diffraction peaks due to random structure, as shown in Figure 2.[35]

A broad peak is observed in the range of 20° to 30°, centered at 22.7°, which reflects the amorphous structure of the NC. Ag-100 and Ag-200 show no apparent differences from the NC XRD pattern, as seen in Figure 2. Ag-300 shows a less intense (111) diffraction peak of FCC silver observed at 2θ = 37.97°. With the increase in the amount of vacuum-filtered silver nanowires on the NC surface, the intensity of the (111) peak increases significantly along with the less intense (200) peak positioned at 2θ = 44.23°. Finally, Ag-3000 exhibits all five FCC silver peaks (JCPDS file no. 04-0783). The lattice constant of the sample is around 4.09 Å.

Surface FESEM images are analyzed to see the AgNWs coated NC paper distribution, respectively. The surface of the

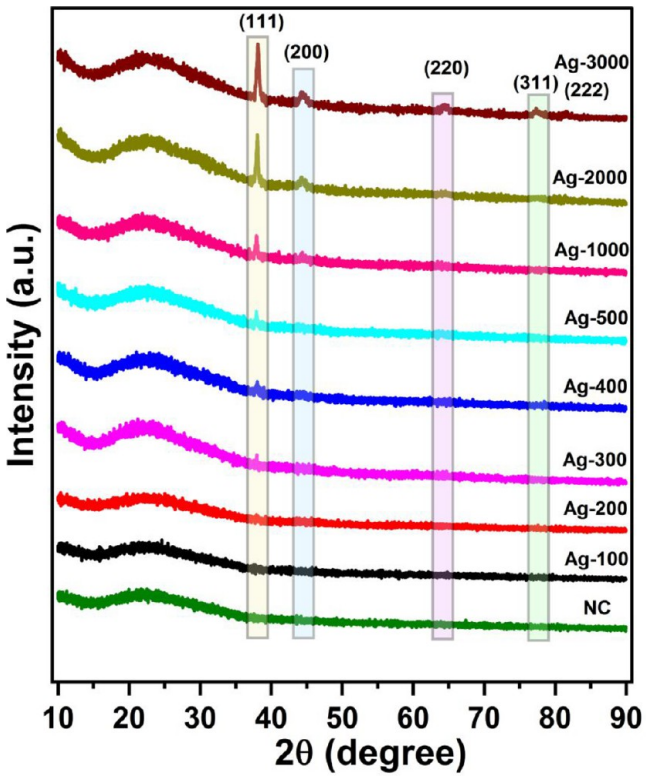

Figure 2. XRD patterns obtained for neat and AgNW coated NC papers.

neat NC paper reveals uniform porous and corrugated lotus leaf surface nature as shown in Figure 3a. As observed in Figure 3b, the Ag-100 surface shows few nanowires distributed randomly on the hierarchical porous structure of the NC paper. As more AgNWs solution is vacuum filtered on the NC paper, long nanowires align along the plane and form an interconnected network. The interconnected NWs form a complete layer on the corrugated and porous network, making it a 2D-in planar structure as seen in Figure 3d. Once a layer is formed on the porous surface, AgNWs stack on the layer, making it a dense 3D like structure with reduced porosity as seen in Figure 3e. The structure becomes denser and covers almost all NC porous structures, as seen in the Ag-3000 sample. The EDS mapping is carried out for Ag-2000 to visualize the distribution of Ag and C elements in the coated paper. Figure 3g′,g′′ depicts Ag and C contribution to the overall coated paper. The figures suggest the uniform coating of AgNW over the NC paper.

The cross-sectional images show coated nanowires placed on the NC base, as depicted in Figure 4. Figure 4a−c shows a sequential order of the cross-sectional image taken for Ag-2000. The average thickness of the NC is calculated to be 135 ± 0.8 μm, and a minimal layer coating thickness is observed. To avoid microscopic edge bending and find the exact thickness of the AgNWs layer, we used commercially available epoxy and pasted it on both sides of coated paper, as shown in Figure 4f. The average AgNW layer thickness is found to be 0.69 ± 0.11 μm for the Ag-3000 sample. While maximum nanowires align in the plane on the porous structure, some of the nanowires pass through the filter membrane (0.22 μm pore size, while the average diameter of the nanowires was about 53 nm). As shown in Figure 4e, the surface of the NC exhibits a regular humpy and wavy arrangement, and nanowires are

https://doi.org/10.1021/acsomega.2c05204
ACS Omega 2022, 7, 41426−41436

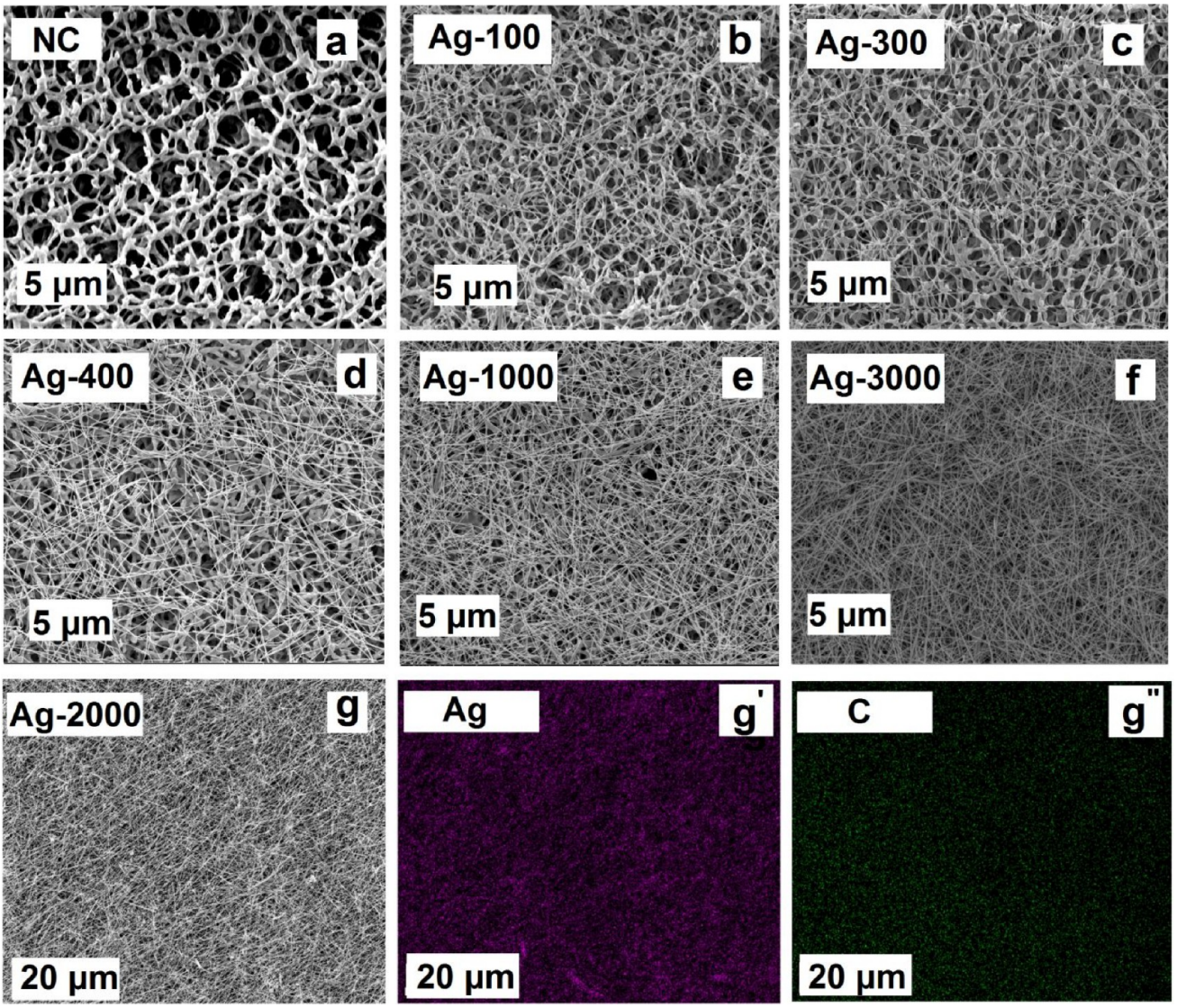

Figure 3. Surface FESEM images of (a) pristine NC paper, (b–f) Ag-100, Ag-300, Ag-400, Ag-1000, and Ag-3000 showing nanowires distribution on the NC paper, (g) surface image of Ag-2000 used for EDS elemental mapping of Ag (g′) and C (g′′) content on the coated paper.

rolled over that surface, filling the cavity present in it. In this way, self-assembled nanowires fill the gap or pore present in the NC surface and make it a 3D interconnected hybrid structure.

2.2.2. Electrical Property Measurement. The electrical conductivity of the AgNW-coated NC paper composites is measured using the linear four-probe method. From the linear dependence of the obtained voltage (V) for the input current (I) (Figure 5a), resistance (R) is evaluated. The geometrical correction factor is considered to calculate electrical resistivity due to insulating the NC bottom layer.

$$\rho = \frac{\pi}{\ln 2}\left(\frac{V}{I}\right) \times t \times f = 4.5324\left(\frac{V}{I}\right) \times t \times f \quad (1)$$

where ρ and t are the electrical resistivity and thickness of the coating of the samples, respectively. f is the geometrical correction factor which is a function of (d/s), d being the sample diameter, and s is the distance between the probes (0.2 mm).

The sheet resistance $\left(R_s = \frac{\rho}{t}\right)$ of the coated papers decreases with an increase in AgNW loading in the coated paper. While the Ag-100 sample shows a sheet resistance of 79.5 Ω/sq, and Ag-3000 shows the lowest sheet resistance of 0.85 Ω/sq as shown in Figure 5b. A sharp fall is observed from 54.3 Ω/sq to 14.4 Ω/sq for the Ag-300 sample, which may be due to the formation of the percolated network.

Electrical conductivity $\left(\sigma_{dc} = \frac{1}{\rho}\right)$ of the prepared samples follows a similar trend to sheet resistance but in an opposite sense, as depicted in Figure 5b. Ag-100 shows electrical conductivity of 92 S/m due to the randomly aligned silver nanowires network across the NC matrix. However, due to an interconnected conductive pathway formed due to self-assembled AgNWs, the conductivity manifested multiple times taking up to 511 S/m for Ag-300. As an electrical network is formed on the insulating surface, the addition of more AgNWs to the network enhances the overall conductivity. The linear enhancement in electrical conductivity (1071 S/m, 1828 S/m, and 3976 S/m for Ag-500, Ag-1000,

https://doi.org/10.1021/acsomega.2c05204
ACS Omega 2022, 7, 41426–41436

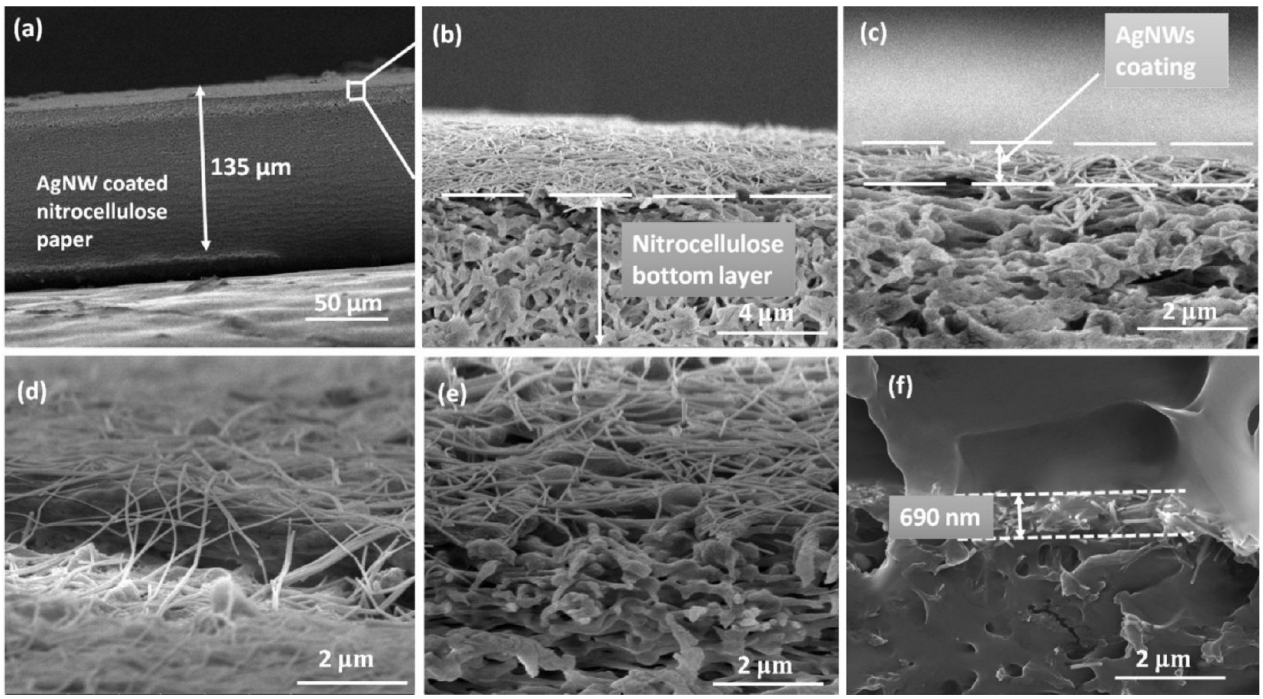

Figure 4. Cross-sectional FESEM images of AgNW coated NC paper (a), (b), and (c) showing silver nanowires coating on NC bottom matrix, (d) shows random NWs intersecting and rolling over each over on the membrane surface, (e) self-assembly of AgNWs over the regular, porous, and corrugated NC structure, and (f) AgNW coated NC paper dipped in epoxy for thickness measurement.

and Ag-2000, respectively) can be attributed to the dense AgNWs network formed by the vacuum filtration. Ag-3000 exhibits the highest electrical conductivity, about 8603 S/m.

2.2.3. EMI Shielding Measurement. EMI shielding properties of the coated conductive papers are carried out using a microwave vector network analyzer in the X-band region (8−12 GHz). The total EMI shielding effectiveness (SE_T) can be expressed in terms of shielding due to absorption (SE_A) and shielding due to reflection (SE_R).

$$SE_T = SE_R + SE_A \tag{2}$$

SE_R, SE_A, and SE_T can be written in terms of S-parameters as

$$SE_R = 10\log\left(\frac{1}{1 - |S_{11}|^2}\right) \tag{3}$$

$$SE_A = 10\log\left(\frac{1 - |S_{11}|^2}{|S_{21}|^2}\right) \tag{4}$$

$$SE_T = 10\log\left(\frac{1}{|S_{21}|^2}\right) \tag{5}$$

where S_{11} and S_{21} are the complex reflection and transmission coefficients, respectively.

EMI shielding efficiency (%) can be derived from shielding effectiveness (dB) as

$$\text{shielding efficiency (\%)} = 100 - \left(\frac{1}{10^{SE_T/10}}\right) \times 100 \tag{6}$$

Figure 5c depicts the total EMI SE (SE_T) measured in the X-band region (8−12 GHz), showing quasi-linear behavior, where EMI SE decreases with an increase in frequency.[36] It may be noted that Ag-3000 achieved a maximum of 75 dB shielding at 8 GHz.

Bare NC paper offers a very minimal average EMI SE of about 0.15 dB. In contrast, with the addition of AgNWs content, coated papers show an improvised average EMI SE reaching around 22.7 ± 0.9 dB for Ag-300, blocking more than 99% of the net radiation, surpassing the commercial requirement application (SE ≥ 20 dB).[1,18,37] The improvised SE_T can be attributed to the electrical conductivity of the coated paper as shown in Figure 5b. Although there is an appropriate increment in electrical conductivity (511 S/m to 812 S/m), Ag-400 paper displays an exceptional increment in SE_T, achieving 54.1 ± 3.4 dB and blocking nearly 99.9996% of the initial power. Despite adding more nanowires to the rough surface of NC, Ag-500 and Ag-1000 did not exhibit much difference in SE_T, reaching around 56 and 57 dB, respectively. With a further doubling of the volume of silver nanowires solution, SE_T increases substantially, extending to 63.2 ± 3.4 dB and 69.2 ± 3.4 dB for Ag-2000 and Ag-3000, respectively, blocking almost all (∼99.99999%) of original incident radiation.

Figure 5d presents the contribution of reflection and absorption to the total EMI shielding. It is evident from the figure that shielding due to absorption (SE_A) is more dominant than shielding due to reflection (SE_R) for all the samples. For example, in the case of Ag-100, the average SE_R has a value of 3.2 ± 0.2 dB, which corresponds to more than 52% of incident power reflected from the surface. SE_A has a value of 8 ± 0.4 dB, which corresponds to 84% of the power absorbed from the unreflected power by the AgNW networks. Henceforth, combining these two, about 92% of the incoming radiations are prevented from coming out of the shield. Shielding due to reflection (SE_R) attains a maximum of 23.7 ± 2 dB for Ag-3000, while its absorption contribution is around 45.5 ± 2.1 dB at 10 GHz. One can observe a steep increase in shielding for the Ag-400 sample due to enhanced absorption (SE_A), which jumps from 14 ± 0.5 dB (for Ag-300) to 42 ± 2.9 dB, whereas

https://doi.org/10.1021/acsomega.2c05204
ACS Omega 2022, 7, 41426−41436

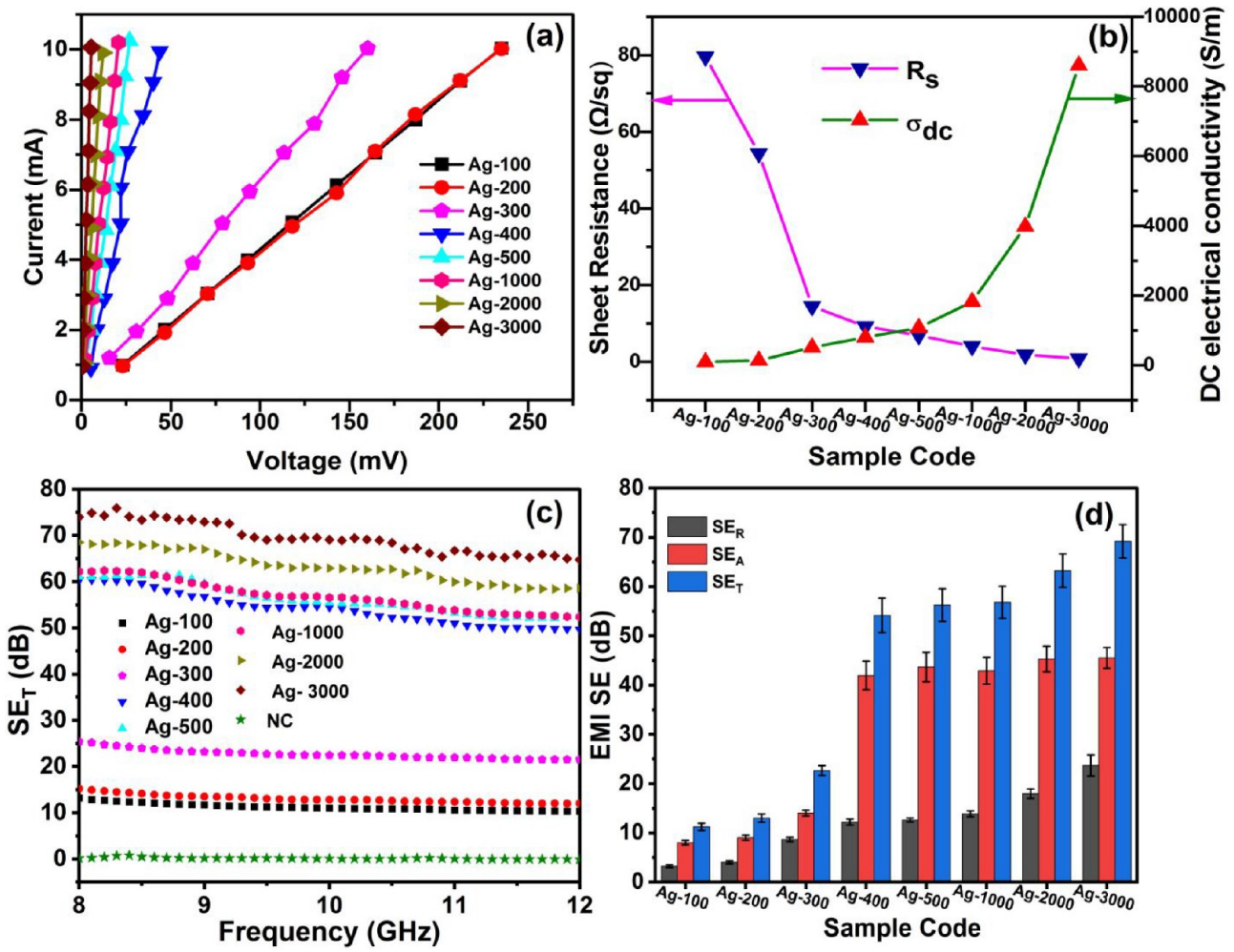

Figure 5. (a) Current (I)−voltage (V) data, (b) sheet resistance (R_s) and DC electrical conductivity (σ_{dc}) values obtained for all coated samples, (c) SE_T recorded for all samples in the X-band region (8−12 GHz), and (d) relative contribution of SE_R and SE_A to total EMI SE measured.

SE_R merely increases from 8.6 ± 0.4 dB (for Ag-300) to 12.2 ± 0.5 dB. Though $SE_A > SE_R$, it may be noted that the reflectivity for Ag-300 is 0.86 (0.94 for Ag-400) while the absorptivity is 0.13 for Ag-300 (0.059996 for Ag-400).

2.2.3.1. Effective Material Properties. A plane-wave-based theory for a multilayered system (air-AgNW-NC-air combination) is employed to understand the shielding mechanism. The electric field radiation in the $(n+1)^{th}$ layer entering from the n^{th} layer can be expressed in a matrix form as

$$\begin{bmatrix} E_{n+1}^{+} \\ E_{n+1}^{-} \end{bmatrix} = \frac{1}{T_{n,n+1}} \begin{bmatrix} 1 & R_{n,n+1} \\ R_{n,n+1} & 1 \end{bmatrix} \begin{bmatrix} e^{-\gamma_n d_n} & 0 \\ 0 & e^{+\gamma_n d_n} \end{bmatrix} \begin{bmatrix} E_n^{+} \\ E_n^{-} \end{bmatrix} \quad (7)$$

where E_j^{+} and E_j^{-} are the electric field amplitudes of incoming and outgoing radiation in the j^{th} medium. γ_j, and d_j are the complex propagation factor and thickness of the j^{th} layer, respectively. The complex reflection and transmission coefficient can be expressed as

$$R_{i,j} = \frac{\frac{\mu_i}{\varepsilon_i} - \frac{\mu_j}{\varepsilon_j}}{\frac{\mu_i}{\varepsilon_i} + \frac{\mu_j}{\varepsilon_j}} \text{and} T_{i,j} = \frac{2\frac{\mu_i}{\varepsilon_i}}{\frac{\mu_i}{\varepsilon_i} + \frac{\mu_j}{\varepsilon_j}} \quad (8)$$

Here $\mu = \mu' - j\mu''$ and $\varepsilon = \varepsilon' - j\varepsilon''$ are the magnetic permeability and electric permittivity of the medium, respectively.

The reflectivity (R) and transmissivity (T) can be derived as

$$R = \left|\frac{E_1^{-}}{E_1^{+}}\right|^2 \text{and} T = \left|\frac{E_n^{+}}{E_1^{+}}\right|^2 \quad (9)$$

SE_R and SE_A can be derived as

$$SE_R = 10\log\left(\frac{1}{1-R}\right) \text{and} SE_A = 10\log\left(\frac{1-R}{T}\right) \quad (10)$$

The effective material properties of the individual layer are extracted by matching the experimentally obtained values with the calculated values. The effective conductivity (σ_{ac}) and imaginary part of permeability (μ'') values of AgNWs network are extracted with varying frequency by assuming the value of the dielectric constant of AgNWs and nitrocellulose layer as 1 and 3.4, respectively, and is depicted schematically in Figure S7.

The effective conductivity (σ_{ac}) is directly related to dielectric loss and explains the polarization of the mobile charges. The dielectric loss includes interfacial loss (due to the collection of charge carriers at the interface), conductance loss, defect dipole polarization, and space-charge polarization. The

https://doi.org/10.1021/acsomega.2c05204
ACS Omega 2022, 7, 41426−41436

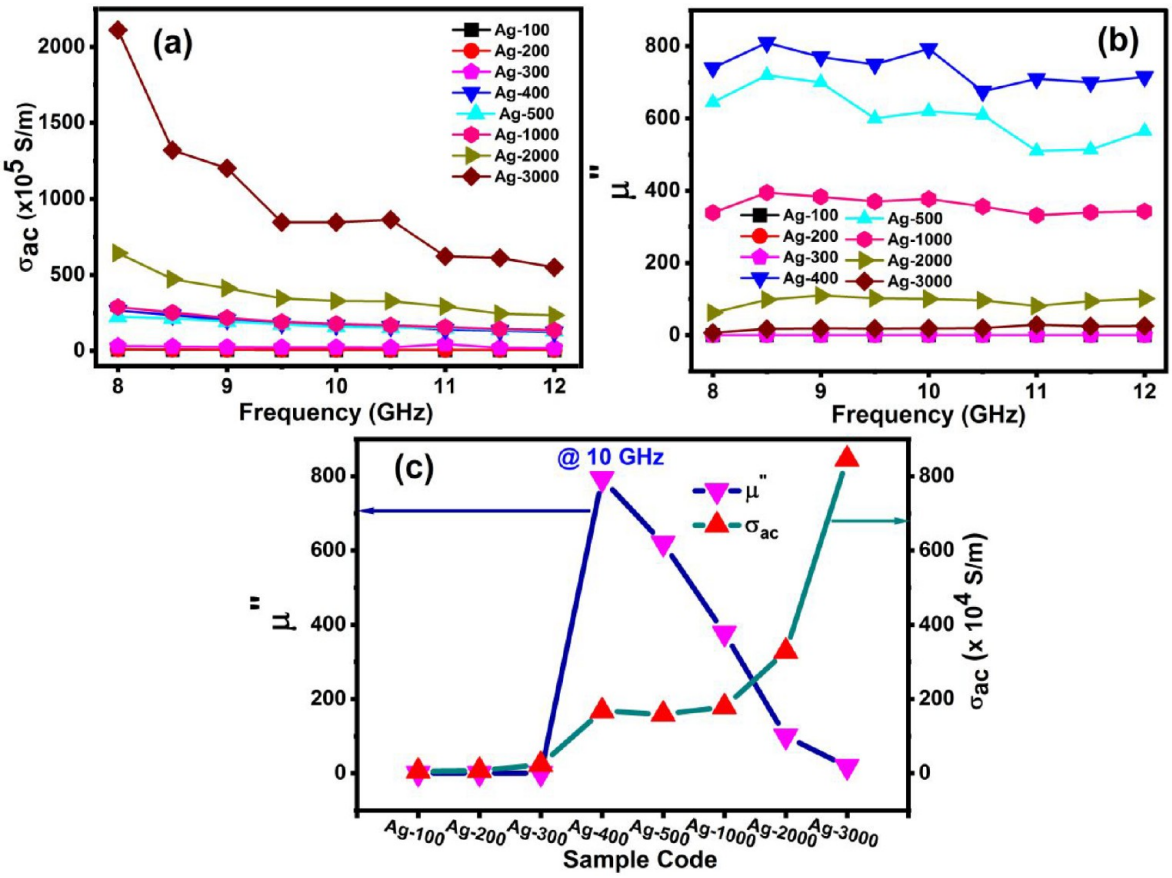

Figure 6. Extracted effective values of AgNWs network (a) σ_{ac} and (b) μ'' for all samples as a function of frequency, (c) σ_{ac} and μ'' values for different samples at 10 GHz.

extracted values of σ_{ac} of the coated AgNWs exhibit substantial enhancement with the increase in concentration which increases monotonously from 5.4×10^4 S/m to 8.46×10^6 S/m for Ag-100 to Ag-3000 samples at 10 GHz as shown in Figure 6c. The linear enhancement is attributed to the formation of well interconnected nanowires due to vacuum filtration coating. However, we observe a noticeable decrease in σ_{ac} as the frequency increases for each corresponding sample, as depicted in Figure 6a. For instance, the value for Ag-3000 is around 2.1×10^7 S/m at 8 GHz, reducing to 5.5×10^6 S/m at 12 GHz.

Surprisingly, one can observe a considerable involvement of magnetic loss (μ'') in the samples. However, the parameter behaved with frequency-independent behavior, which remained relatively constant over the X-band frequency range for a particular sample as shown in Figure 6b. It is noticed that there is a sharp increase in μ'' from zero for Ag-100, Ag-200, and Ag-300 samples to 793 for Ag-400. It gradually decreases to around 18.5 for Ag-3000, as seen in Figure 6c. Though there is no presence of magnetic impurities in the samples, this can be explained as the effect of conducting network formed by AgNWs on porous structure. As seen from FESEM images of Ag-100 to Ag-300 samples, there is no interconnected network. Only a few isolated nanowires are present on the porous surface. This does not contribute to closed current loops. As Kumaran et al. proposed, a sufficient amount of nanofillers should be present to form circulating current-carrying loops generating magnetic loss.[38] The sharp change in μ'' from 0 to 793 is associated with the formation of interconnected networks that results in the loop currents giving rise to magnetic moments. This is further helped by the porosity of NC paper, which allows the circulating current even in its bulk region. As NWs stack on each other, loop currents start canceling each other, effectively reducing the value of μ''. Therefore, μ'' decreases monotonously to 18 for the Ag-3000 sample (Table 1).

Table 1. Extracted Values of AC Conductivity and Imaginary Part of Permeability Value of AgNW Layer at 10 GHz for Different Samples

sample code	AC conductivity (σ_{ac}) (S/m)	imaginary part of permeability (μ'')
Ag-100	54359	0
Ag-200	73600	0
Ag-300	230700	0
Ag-400	1679535	793
Ag-500	1587918	620
Ag-1000	1786185	377
Ag-2000	3283000	100
Ag-3000	8459000	18

The underlying EMI shielding mechanism of AgNWs coated NC paper is explained schematically in Figure 7. When a high-frequency EM wave is incident on the hybrid paper, highly conductive nanowires on the surface reflect a considerable part of its energy due to a substantial impedance mismatch between material and free space.[5,8] The porous NC surface aids in reducing the impedance mismatch by allowing EM waves to go

https://doi.org/10.1021/acsomega.2c05204
ACS Omega 2022, 7, 41426−41436

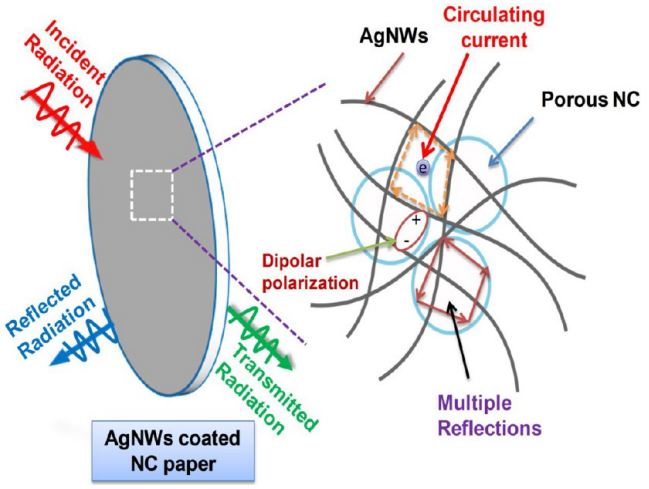

Figure 7. EMI shielding mechanism of AgNWs coated NC paper; enlarged view of AgNWs coated on the porous structure leading to different mechanisms such as multiple reflections, magnetic loss due to circulating current loops, and dipolar polarization.

inside.[10] As the EM wave goes inside the material, its amplitude decreases exponentially depending on the skin depth of the material. The 3D conductive composite paper promotes dipolar polarization leading to dielectric loss at the interfaces and giving rise to eddy current loss as heat energy. The nanowires filled in the porous NC matrix with completely different conductivities lead to the formation of many micro capacitors regionally, which ultimately reduce EM wave energy by accumulating and migrating space charges. Due to these collective efforts, microwaves either get reflected or absorbed inside the material while only a few get passed through it.[39]

The EMI shielding performance of our fabricated AgNWs coated NC paper can be compared qualitatively with the recently reported works on coated paper/film/membrane by taking specific EMI shielding (SE/t) to eliminate the substrate thickness factor into consideration. As the substrate does not contribute much to effective EMI SE, only coating thickness is considered while calculating SE/t, as displayed in Table 2. AgNWs coated NC paper surpasses EMI shielding performances of dip-coated [AgNW-cellulose paper,[26] AgNW-MWCNT-cellulose,[27] AgNW-NiNP-cellulose,[28] MWCNT-cellulose paper,[40] H-AgNW-cellulose paper,[41] carbon nanofiber-CFP,[42] AgNW-electrospun PVDF[43]], Spray-coated [AgNW-electrospun PVDF,[43] $Ti_3C_2T_x$-AgNW-silk fabric,[44] 9- PEI/rGO,[45] AgNP-CF paper,[46] $Ti_3C_2T_x$ in bacterial cellulose (BC)[47]], and vacuum filtration coated $Ti_3C_2T_x$-cellulose paper.[29] Despite having AgNWs coating thickness of 0.69 μm and area density of 0.041 mg/cm^2, AgNWs coated NC paper achieved SE/t of 1005797 dB/cm surpassing the SE/t of dip-coated AgNW in CFP (50103 dB/cm), spray coated $Ti_3C_2T_x$/AgNW on silk textile (840000 dB/cm), vacuum filtration coated of $Ti_3C_2T_x$ on CFP (24500 dB/cm). Thus, a highly conductive AgNWs network self-assembled under vacuum on NC filter paper can be an ideal candidate for high-performance EMI shielding for miniaturized electronics applications.

3. CONCLUSION

A series of AgNWs coated NC filter papers were fabricated using a simple and quickly processed vacuum-assisted filtration method by varying the filtrate volume. Structural and EMI shielding properties of the fabricated paper were investigated systematically. FESEM images revealed the lotus leaf-like rough and porous structure of the NC paper where long and thin 1D nanowires were interwoven and made a dense layer on the surface. Due to the strong interconnected AgNW network, the coated paper exhibited an electrical conductivity of 8603 S/m. It is observed that the conductive networks due to silver nanowires result in scattering, effectively absorbing the EM radiation. The conducting networks form circulating currents resulting in magnetic loss. The combination of conduction loss and magnetic loss coupled with enhanced conductivity resulted in an excellent EMI SE of 69 dB with a specific EMI SE (SE/t) of 1005797 dB/cm over the X-band region. This achievement is realized despite a minimal silver nanowires coating thickness of 0.69 μm and an area density of 0.041 mg/cm^2. Our results proved that a simple, quickly processed vacuum-assisted filtration AgNWs coating can achieve ultrahigh EMI shielding.

4. EXPERIMENTAL SECTION

4.1. Materials. Ultrapure silver nitrate ($AgNO_3$, purity >99.5%), sodium chloride (NaCl, purity >99.5%), and

Table 2. Comparison with Reported EMI Shielding Performance of the Coated Samples by Various Coating Methods

method	materials	coating thickness (μm)	frequency range (GHz)	EMI SE (dB)	specific EMI SE (dB/cm)	ref
dip coating	AgNW in CFP	9.7	0.5−1	48.6	50103	26
	MWCNT in CFP	15.6	0.5−1	20.1	12884	40
	AgNW/MWCNT in CFP	6.5	0.5−1	23.8	36615	27
	AgNW/NiNP on CFP	77	8.2−12.4	88.4	11480	28
	H-AgNW/cellulose	15.6	8.2−12.4	46.1	29487	41
	AgNW/electrospun PVDF membrane	40	8.2−12.4	107.2	26800	43
	carbon nano fiber/CFP	12.7	0.5−1	24.6	19370	42
spray coating	AgNW on electrospun PVDF membrane	∼1	8.2−12.4	33.4	334000	43
	$Ti_3C_2T_x$/AgNW on silk textile	0.5	8.2−12.4	42	840000	44
	PEI/rGO	6	8.2−12.4	29	48300	45
	AgNP/Carbon fiber	61	8−12	102	16721	46
	$Ti_3C_2T_x$ in bacterial cellulose	7.71	8.2−12.4	60	77821	47
vacuum filtration coating	$Ti_3C_2T_x$ on CFP	12	8.2−12.4	29.4	24500	29
	AgNW on NC filter paper	**0.69**	**8−12**	**69.4**	1005797	**this work**

https://doi.org/10.1021/acsomega.2c05204
ACS Omega 2022, 7, 41426−41436

ethylene glycol (EG, purity >99%) were purchased from Sisco Research Laboratory Chemicals, India. Poly (vinylpyrrolidone) (MW ∼ 130 K) and potassium bromide (KBr, purity >99%) were purchased from Sigma-Aldrich, U.S.A. Commercial NC filter papers (135 μm thickness, 47 mm diameter and 0.22 μm pore size) were purchased from Riviera Glass Pvt. Ltd., India. Deionized (DI) water with a resistivity of 18.2 MΩ·cm was collected from the laboratory facility. All other chemicals used were of analytical grade and without any further purification.

4.2. Synthesis of Silver Nanowires (AgNWs). AgNWs were synthesized by the modified polyol method as reported by Hu et al. with some modifications and shown schematically in Figure S1a.[48] Typically, 40 mL of EG was taken in a round-bottomed flask and heated at 160 °C to remove any water content. Then, 1.30 g of PVP and 0.02 g of KBr were added to the flask with continuous magnetic stirring. About 0.1 g of silver chloride powder (AgCl), which was prepared by adding 0.1 M $AgNO_3$ solution to NaCl solution, was added to the above flask for initial nucleation of Ag^0 seeds. About 0.44 g of $AgNO_3$ powder was mixed with 10 mL of preheated EG and added slowly at a rate of 200 μL/min with the help of a dropper. The flask was capped and left undisturbed for 30 min to complete the growth of nanowires. The flask was removed and cooled naturally. About 150 mL of acetone was added, and the flask was left undisturbed overnight. The settled AgNWs were collected after pipetting out the supernatant solution. The nanowires were further centrifuged with ethanol and water to remove short and thick nanowires. Finally, AgNWs were stored with ethanol for future use.

4.3. Fabrication of Silver Nanowires Coated Nitrocellulose Paper. AgNW solutions were centrifuged before use to avoid any agglomerations. As depicted in Figure S1b, an adequate amount of DI water was added to make an AgNWs solution with a concentration of 0.7 mg/mL. Different volumes (100 μL−3 mL) of AgNWs solution with water were vacuum filtered on the commercial cellulose nitrate filter paper. The vacuum-filtered paper was dried overnight at room temperature. The dried films were given names according to the volume of silver nanowires solutions used, such as Ag-100 (for 100 μL), Ag-200 (for 200 μL) to Ag-3000 (for 3 mL), respectively. The photographs of the films are shown in Figure S1c, displaying observable color changes to the coated paper.

4.4. Characterization. The crystalline structure of the silver nanowires was characterized by X-ray diffraction (XRD) (Bruker D8 Discover AXS powder X-ray diffractometer, Germany operating voltage 40 kV, current 40 mA) with a step size of 0.01° in the range from 10° to 90°. The 3D morphology of the nanowires was obtained by field emission scanning electron microscope (FEI INSPECT-F50, U.S.A.) with an operating voltage between 5 and 30 kV. The elemental composition of the nanowires was calculated by taking energy-dispersive X-ray analysis (EDX) spectra. 2D morphology and selected area electron diffraction (SAED) pattern were taken from a transmission electron microscope (TEM, TECNAI-G20, U.S.A.) with an operating voltage of 200 kV. The length and diameter calculations were performed using ImageJ software. The optical measurements were done by dispersing a small amount of the AgNWs solution in water and measuring the absorbance UV−visible spectra (JASCO V-570 UV−vis spectrometer) in the wavelength region between 300 and 800 nm.

The morphology and thickness of coated papers were characterized by FESEM (FEI INSPECT-F50). The structure and phase of the samples were characterized by obtaining XRD patterns. DC electrical conductivity of the coated samples was performed using a four-point probe (Model- DFP-RM-200, SES Instruments Pvt. Ltd., India) at room temperature. EMI shielding performance was evaluated by measuring four scattering parameters (S_{11}, S_{12}, S_{21}, and S_{22}) using an Agilent Microwave Vector Network Analyzer (N5230C, Keysight Technologies, U.S.A.) with the waveguide transmission line as demonstrated in Figure S6. Samples were cut into little larger than X-band (8 to 12 GHz) dimensions (22.86 × 10.16 mm) for measurements.

■ ASSOCIATED CONTENT

Supporting Information

The Supporting Information is available free of charge at https://pubs.acs.org/doi/10.1021/acsomega.2c05204.

Figures (S1−S7): schematic diagrams of synthesis and fabrication method; photos of the coated samples; FESEM images of AgNWs; Distribution of diameter and length of AgNWs; EDAX and SAED pattern obtained from AgNWs; EDAX spectra obtained for Ag-300 sample; photo of the experimental setup for measuring EMI shielding; schematics of the plane-wave theory model adopted for the extraction of the parameters (PDF)

■ AUTHOR INFORMATION

Corresponding Author

Subramanian Venkatachalam − *Microwave Laboratory, Department of Physics, Indian Institute of Technology Madras, Chennai, Tamil Nadu 600036, India*; Email: manianvs@iitm.ac.in

Authors

Raghunath Sahoo − *Microwave Laboratory, Department of Physics, Indian Institute of Technology Madras, Chennai, Tamil Nadu 600036, India; Alternative Energy and Nanotechnology Laboratory, Department of Physics, Indian Institute of Technology Madras, Chennai, Tamil Nadu 600036, India;* orcid.org/0000-0001-6225-3263

Ramaprabhu Sundara − *Alternative Energy and Nanotechnology Laboratory, Department of Physics, Indian Institute of Technology Madras, Chennai, Tamil Nadu 600036, India;* orcid.org/0000-0002-7960-9470

Complete contact information is available at: https://pubs.acs.org/10.1021/acsomega.2c05204

Notes

The authors declare no competing financial interest.

■ ACKNOWLEDGMENTS

The authors would like to thank Mr. Govinda Chandra Behera for taking cross-sectional FESEM images and Mr. Asapu Vinaya Kumar for helping in writing MATLAB code.

■ REFERENCES

(1) Geetha, S.; Satheesh Kumar, K. K.; Rao, C. R. K.; Vijayan, M.; Trivedi, D. C. EMI Shielding: Methods and Materials-A Review. *J. Appl. Polym. Sci.* **2009**, *112* (4), 2073−2086.

(2) Kang, J.; Kim, D.; Kim, Y.; Choi, J.-B.; Hong, B. H.; Kim, S. W. High-Performance near-Field Electromagnetic Wave Attenuation in Ultra-Thin and Transparent Graphene Films. *2D Mater.* **2017**, *4* (2), 025003.

(3) Singh, S.; Kapoor, N. Health Implications of Electromagnetic Fields, Mechanisms of Action, and Research Needs. *Adv. Biol.* **2014**, *2014*, 1−24.
(4) Carpenter, D. O. Human Disease Resulting from Exposure to Electromagnetic Fields. *Rev. Environ. Health* **2013**, *28* (4), 159−172.
(5) Menon, A. V.; Madras, G.; Bose, S. Phase Specific Dispersion of Functional Nanoparticles in Soft Nanocomposites Resulting in Enhanced Electromagnetic Screening Ability Dominated by Absorption. *Phys. Chem. Chem. Phys.* **2017**, *19* (1), 467−479.
(6) Chen, Y.; Yang, Y.; Xiong, Y.; Zhang, L.; Xu, W.; Duan, G.; Mei, C.; Jiang, S.; Rui, Z.; Zhang, K. Porous Aerogel and Sponge Composites: Assisted by Novel Nanomaterials for Electromagnetic Interference Shielding. *Nano Today* **2021**, *38*, 101204.
(7) Eswaraiah, V.; Sankaranarayanan, V.; Ramaprabhu, S. Functionalized Graphene-PVDF Foam Composites for EMI Shielding. *Macromol. Mater. Eng.* **2011**, *296* (10), 894−898.
(8) Kumaran, R.; Alagar, M.; Dinesh Kumar, S.; Subramanian, V.; Dinakaran, K. Ag Induced Electromagnetic Interference Shielding of Ag-Graphite/PVDF Flexible Nanocomposites Thinfilms. *Appl. Phys. Lett.* **2015**, *107* (11), 113107.
(9) Nallabothula, H.; Bhattacharjee, Y.; Samantara, L.; Bose, S. Processing-Mediated Different States of Dispersion of Multiwalled Carbon Nanotubes in PDMS Nanocomposites Influence EMI Shielding Performance. *ACS Omega* **2019**, *4* (1), 1781−1790.
(10) Guo, H.; Li, Y.; Ji, Y.; Chen, Y.; Liu, K.; Shen, B.; He, S.; Duan, G.; Han, J.; Jiang, S. Highly Flexible Carbon Nanotubes/Aramid Nanofibers Composite Papers with Ordered and Layered Structures for Efficient Electromagnetic Interference Shielding. *Compos. Commun.* **2021**, *27* (July), 100879.
(11) Chen, Y.; Zhang, L.; Mei, C.; Li, Y.; Duan, G.; Agarwal, S.; Greiner, A.; Ma, C.; Jiang, S. Wood-Inspired Anisotropic Cellulose Nanofibril Composite Sponges for Multifunctional Applications. *ACS Appl. Mater. Interfaces* **2020**, *12* (31), 35513−35522.
(12) Chen, Y.; Luo, H.; Guo, H.; Liu, K.; Mei, C.; Li, Y.; Duan, G.; He, S.; Han, J.; Zheng, J.; E, S.; Jiang, S. Anisotropic Cellulose Nanofibril Composite Sponges for Electromagnetic Interference Shielding with Low Reflection Loss. *Carbohydr. Polym.* **2022**, *276*, 118799.
(13) Guo, H.; Chen, Y.; Li, Y.; Zhou, W.; Xu, W.; Pang, L.; Fan, X.; Jiang, S. Electrospun Fibrous Materials and Their Applications for Electromagnetic Interference Shielding: A Review. *Compos. Part A Appl. Sci. Manuf.* **2021**, *143*, 106309.
(14) Guo, H.; Wang, F.; Luo, H.; Li, Y.; Lou, Z.; Ji, Y.; Liu, X.; Shen, B.; Peng, Y.; Liu, K.; Jiang, S. Flexible TaC/C Electrospun Non-Woven Fabrics with Multiple Spatial-Scale Conductive Frameworks for Efficient Electromagnetic Interference Shielding. *Compos. Part A Appl. Sci. Manuf.* **2021**, *151*, 106662.
(15) Guo, H.; Zheng, M.; Ma, X.; Cao, R.; Liu, K.; Yang, W.; Jian, S.; Jiang, S.; Duan, G. Electrospun TaC/Fe3C-Fe Carbon Composite Fabrics for High Efficiency of Electromagnetic Interference Shielding. *Compos. Commun.* **2022**, *31*, 101130.
(16) Xu, F.; Shen, W.; Xu, W.; Li, J.; Song, W.Silver Nanowires as Shielding Materials. In *Advanced Materials for Electromagnetic Shielding*; Jaroszewski, M., Thomas, S., Rane, A. V., Eds.; John Wiley & Sons, Inc.: Hoboken, NJ, 2018; pp 289−304. DOI: 10.1002/9781119128625.ch13.
(17) Yu, Y.-H.; Ma, C.-C. M.; Teng, C.-C.; Huang, Y.-L.; Lee, S.-H.; Wang, I.; Wei, M.-H. Electrical, Morphological, and Electromagnetic Interference Shielding Properties of Silver Nanowires and Nanoparticles Conductive Composites. *Mater. Chem. Phys.* **2012**, *136* (2−3), 334−340.
(18) Hu, M.; Gao, J.; Dong, Y.; Li, K.; Shan, G.; Yang, S.; Li, R. K. Y. Flexible Transparent PES/Silver Nanowires/PET Sandwich-Structured Film for High-Efficiency Electromagnetic Interference Shielding. *Langmuir* **2012**, *28* (18), 7101−7106.
(19) Ma, J.; Zhan, M.; Wang, K. Ultralightweight Silver Nanowires Hybrid Polyimide Composite Foams for High-Performance Electromagnetic Interference Shielding. *ACS Appl. Mater. Interfaces* **2015**, *7* (1), 563−576.
(20) Fang, F.; Li, Y.-Q.; Xiao, H.-M.; Hu, N.; Fu, S.-Y. Layer-Structured Silver Nanowire/Polyaniline Composite Film as a High Performance X-Band EMI Shielding Material. *J. Mater. Chem. C* **2016**, *4* (19), 4193−4203.
(21) Arjmand, M.; Moud, A. A.; Li, Y.; Sundararaj, U. Outstanding Electromagnetic Interference Shielding of Silver Nanowires: Comparison with Carbon Nanotubes. *RSC Adv.* **2015**, *5* (70), 56590−56598.
(22) Liang, C.; Ruan, K.; Zhang, Y.; Gu, J. Multifunctional Flexible Electromagnetic Interference Shielding Silver Nanowires/Cellulose Films with Excellent Thermal Management and Joule Heating Performances. *ACS Appl. Mater. Interfaces* **2020**, *12* (15), 18023−18031.
(23) Chen, Y.; Pang, L.; Li, Y.; Luo, H.; Duan, G.; Mei, C.; Xu, W.; Zhou, W.; Liu, K.; Jiang, S. Ultra-Thin and Highly Flexible Cellulose Nanofiber/Silver Nanowire Conductive Paper for Effective Electromagnetic Interference Shielding. *Compos. Part A Appl. Sci. Manuf.* **2020**, *135* (April), 105960.
(24) Zhou, B.; Li, Q.; Xu, P.; Feng, Y.; Ma, J.; Liu, C.; Shen, C. An Asymmetric Sandwich Structural Cellulose-Based Film with Self-Supported MXene and AgNW Layers for Flexible Electromagnetic Interference Shielding and Thermal Management. *Nanoscale* **2021**, *13* (4), 2378−2388.
(25) Liu, K.; Liu, W.; Li, W.; Duan, Y.; Zhou, K.; Zhang, S.; Ni, S.; Xu, T.; Du, H.; Si, C. Strong and Highly Conductive Cellulose Nanofibril/Silver Nanowires Nanopaper for High Performance Electromagnetic Interference Shielding. *Adv. Compos. Hybrid Mater.* **2022**, *5* (2), 1078−1089.
(26) Lee, T.-W.; Lee, S.-E.; Jeong, Y. G. Highly Effective Electromagnetic Interference Shielding Materials Based on Silver Nanowire/Cellulose Papers. *ACS Appl. Mater. Interfaces* **2016**, *8* (20), 13123−13132.
(27) Choi, H. Y.; Lee, T. W.; Lee, S. E.; Lim, J. D.; Jeong, Y. G. Silver Nanowire/Carbon Nanotube/Cellulose Hybrid Papers for Electrically Conductive and Electromagnetic Interference Shielding Elements. *Compos. Sci. Technol.* **2017**, *150*, 45−53.
(28) Zhan, Y.; Hao, X.; Wang, L.; Jiang, X.; Cheng, Y.; Wang, C.; Meng, Y.; Xia, H.; Chen, Z. Superhydrophobic and Flexible Silver Nanowire-Coated Cellulose Filter Papers with Sputter-Deposited Nickel Nanoparticles for Ultrahigh Electromagnetic Interference Shielding. *ACS Appl. Mater. Interfaces* **2021**, *13*, 14623−14633.
(29) Zhan, Y.; Meng, Y.; Xie, Q. Simple Approach to Fabricate MXene/Cellulose Paper for Electromagnetic Interference Shielding Applications. *J. Appl. Polym. Sci.* **2021**, *138* (25), 50597.
(30) McKeen, L. W.Environmentally Friendly Polymers. *Permeability Properties of Plastics and Elastomers*; Elsevier, 2012; pp 287−304. DOI: 10.1016/B978-1-4377-3469-0.10013-X.
(31) Anju, V. P.Nanocellulose-Based Composites for EMI Shielding Applications. In *Nanocellulose Based Composites for Electronics*; Thomas, S., Pottathara, Y. B., Eds.; Elsevier, 2021; pp 125−161. DOI: 10.1016/B978-0-12-822350-5.00006-0.
(32) Johan, M. R.; Aznan, N. A. K.; Yee, S. T.; Ho, I. H.; Ooi, S. W.; Darman Singho, N.; Aplop, F. Synthesis and Growth Mechanism of Silver Nanowires through Different Mediated Agents (CuCl 2 and NaCl) Polyol Process. *J. Nanomater.* **2014**, *2014*, 105454.
(33) Parente, M.; van Helvert, M.; Hamans, R. F.; Verbroekken, R.; Sinha, R.; Bieberle-Hütter, A.; Baldi, A. Simple and Fast High-Yield Synthesis of Silver Nanowires. *Nano Lett.* **2020**, *20* (8), 5759−5764.
(34) Bergin, S. M.; Chen, Y. H.; Rathmell, A. R.; Charbonneau, P.; Li, Z. Y.; Wiley, B. J. The Effect of Nanowire Length and Diameter on the Properties of Transparent, Conducting Nanowire Films. *Nanoscale* **2012**, *4* (6), 1996−2004.
(35) Costa, M. N.; Veigas, B.; Jacob, J. M.; Santos, D. S.; Gomes, J.; Baptista, P. V.; Martins, R.; Inácio, J.; Fortunato, E. A Low Cost, Safe, Disposable, Rapid and Self-Sustainable Paper-Based Platform for Diagnostic Testing: Lab-on-Paper. *Nanotechnology* **2014**, *25* (9), 094006.
(36) Han, M.; Shuck, C. E.; Rakhmanov, R.; Parchment, D.; Anasori, B.; Koo, C. M.; Friedman, G.; Gogotsi, Y. Beyond Ti 3 C 2 T X:

https://doi.org/10.1021/acsomega.2c05204
ACS Omega 2022, 7, 41426−41436

MXenes for Electromagnetic Interference Shielding. *ACS Nano* **2020**, *14*, 5008−5016.
(37) Ma, J.; Zhan, M.; Wang, K. Ultralightweight Silver Nanowires Hybrid Polyimide Composite Foams for High-Performance Electromagnetic Interference Shielding. *ACS Appl. Mater. Interfaces* **2015**, *7* (1), 563−576.
(38) Kumaran, R.; Kumar, A. V.; Ramaprabhu, S.; Subramanian, V. Absorption-Enhanced EMI Shielding Using Silver Decorated Three-Dimensional Porous Architected Reduced Graphene Oxide in Polybenzoxazine Composites. *New J. Chem.* **2021**, *45* (36), 16939−16948.
(39) Wang, L.; Ma, Z.; Zhang, Y.; Chen, L.; Cao, D.; Gu, J. Polymer-based EMI Shielding Composites with 3D Conductive Networks: A Mini-review. *SusMat* **2021**, *1* (3), 413−431.
(40) Lee, T. W.; Lee, S. E.; Jeong, Y. G. Carbon Nanotube/Cellulose Papers with High Performance in Electric Heating and Electromagnetic Interference Shielding. *Compos. Sci. Technol.* **2016**, *131*, 77−87.
(41) Ren, F.; Guo, H.; Guo, Z. Z.; Jin, Y. L.; Duan, H. J.; Ren, P. G.; Yan, D. X. Highly Bendable and Durable Waterproof Paper for Ultra-High Electromagnetic Interference Shielding. *Polymers (Basel).* **2019**, *11* (9), 1486.
(42) Mondal, S.; Ganguly, S.; Das, P.; Bhawal, P.; Das, T. K.; Nayak, L.; Khastgir, D.; Das, N. C. High-Performance Carbon Nanofiber Coated Cellulose Filter Paper for Electromagnetic Interference Shielding. *Cellulose* **2017**, *24* (11), 5117−5131.
(43) Qian, J.; Zhang, Z. M.; Bao, R. Y.; Liu, Z. Y.; Yang, M. B.; Yang, W. Lightweight Poly (Vinylidene Fluoride)/Silver Nanowires Hybrid Membrane with Different Conductive Network Structure for Electromagnetic Interference Shielding. *Polym. Compos.* **2021**, *42* (1), 522−531.
(44) Liu, L. X.; Chen, W.; Zhang, H. B.; Wang, Q. W.; Guan, F.; Yu, Z. Z. Flexible and Multifunctional Silk Textiles with Biomimetic Leaf-Like MXene/Silver Nanowire Nanostructures for Electromagnetic Interference Shielding, Humidity Monitoring, and Self-Derived Hydrophobicity. *Adv. Funct. Mater.* **2019**, *29* (44), 1905197.
(45) Vallés, C.; Zhang, X.; Cao, J.; Lin, F.; Young, R. J.; Lombardo, A.; Ferrari, A. C.; Burk, L.; Mülhaupt, R.; Kinloch, I. A. Graphene/Polyelectrolyte Layer-by-Layer Coatings for Electromagnetic Interference Shielding. *ACS Appl. Nano Mater.* **2019**, *2* (8), 5272−5281.
(46) Park, J.; Hu, X.; Torfeh, M.; Okoroanyanwu, U.; Arbabi, A.; Watkins, J. J. Exceptional Electromagnetic Shielding Efficiency of Silver Coated Carbon Fiber Fabrics: Via a Roll-to-Roll Spray Coating Process. *J. Mater. Chem. C* **2020**, *8* (32), 11070−11078.
(47) Zhou, Z.; Song, Q.; Huang, B.; Feng, S.; Lu, C. Facile Fabrication of Densely Packed Ti3C2MXene/Nanocellulose Composite Films for Enhancing Electromagnetic Interference Shielding and Electro-/Photothermal Performance. *ACS Nano* **2021**, *15* (7), 12405−12417.
(48) Hu, L.; Kim, H. S.; Lee, J.; Peumans, P.; Cui, Y. Scalable Coating and Properties of Silver Nanowires. *ACS Nano* **2010**, *4* (5), 2955−2963.

https://doi.org/10.1021/acsomega.2c05204
ACS Omega 2022, 7, 41426−41436